JOURNAL OF SOLID STATE CHEMISTRY **134,** 302–311 (1997)
ARTICLE NO. SC977560

Synthesis of a New Ternary Nitride, Fe_4W_2N, with a Unique η-Carbide Structure

K. S. Weil and P. N. Kumta[1]

Department of Materials Science and Engineering, Carnegie Mellon University, Pittsburgh, Pennsylvania 15213

Received July 7, 1997; accepted July 27, 1997

The structure of a new ternary nitride, Fe_4W_2N, prepared using a metal-organic precursor synthesis route, has been determined by Rietveld refinement of the monochromatic X-ray powder diffraction data. The compound crystallizes in a cubic, η-carbide structure, space group $Fd\bar{3}m$ (227), with $Z = 16$ and a lattice parameter of $a = 11.0810(9)$ Å. The refinement converged with $R_{wp} = 0.1273$, $R_p = 0.0709$, $R_I = 0.0478$, and $S = 1.72$. The compound is isostructural with Fe_4W_2C, the ideal structure consisting of eight octahedra of metal atoms, a random mixture of which one-third are iron and two-thirds are tungsten, centered on a diamond cubic lattice and eight regular tetrahedra of iron atoms centered on a second diamond cubic lattice that interpenetrates the first through a $\frac{1}{2},\frac{1}{2},\frac{1}{2}$ unit cell translation. Sixteen additional iron atoms are tetrahedrally coordinated around the iron tetrahedra and sixteen nitrogen atoms surround the metal octahedra in tetrahedral coordination.

INTRODUCTION

In the past 10 years, a growing list of new ternary and higher order nitride compounds have been discovered. In many of these new nitride systems, one of the elements involved is an alkali or alkaline-earth metal, giving rise to an inductive effect whereby the electropositive element stabilizes the formation of ternary transition metal or post-transition metal nitrides (1–3). More recently, several groups in the materials community have focused their attention on the synthesis of ternary transition metal–transition metal nitrides (4, 5). Two of the motivating factors responsible for this interest include the following: (1) these higher order nitride compounds are expected to display different, more complex crystal structures and more exotic magnetic, optical, and electrical properties in comparison to their binary counterparts and (2) to date, the preparation of this type of ternary nitride using traditional approaches has proven to be quite challenging and may require the development of new chemical synthesis techniques, which could eventually be generally applicable for discovering other new compounds. Thus far, the crystal structures of these new ternaries seem to fall predominantly into one of two categories: (1) layered hexagonal or rhombohedral structures such as $FeWN_2$ and $MnMoN_2$ (6), $CrWN_2$ (7), $CoWN_2$ and $NiWN_2$ (8), and $MnWN_2$ (5, 9) or (2) cubic, η-carbide structures such as Fe_3W_3N (10), Co_3W_3N (11), and Fe_3Mo_3N and Co_3Mo_3N (12).

Historically, compounds exhibiting the η-carbide structure attracted attention with the advent of high-speed steels used in the manufacture of cutting tools. Iron–carbon alloys containing molybdenum and/or tungsten were known to form fine ternary carbide precipitates such as Fe_3Mo_3C and Fe_3W_3C, which were suspected to be responsible for the high strength, hardness, and toughness characteristics attributed to this class of tool steels. Since the initial discovery of Fe_3W_3C by Westgren and Phragmen (13) in 1928, a large number of ternary carbides, oxides, and nitrides exhibiting the η-carbide structure have been either isolated or synthesized. The η-carbide structure has two major variants, namely η_1 and η_2, differentiated primarily by their stoichiometry and atomic Wyckoff coordinates (14). The η_1-designated compounds have a composition of M_3T_3C (where M = Fe, Ni, or Co and T = typically Nb, Ta, Mo, and W), in which the M atoms sit on the 32(e) and 16(d) sites of the $Fd\bar{3}m$ space group (origin choice #1), the T atoms sit on the 48(f) positions, and the carbon atoms rest in the 16(c) sites (15). The η_2 structure, on the other hand, has a composition of M_2T_4C and an atomic arrangement nearly identical to that of η_1 except that M atoms on the 16(d) sites are replaced with T atoms, thus yielding the required ratio of T to M atoms of 64 : 32 or 2 : 1 (16). Other derivatives of the η_1 and η_2 structures include compounds such as Co_6W_6C (17) and $Nb_8Zn_4C_3$ (18), in which the carbon atoms respectively occupy either the 8(a) positions solely or the 8(a) and 16(c) sites jointly.

[1] To whom correspondence should be addressed.

0022-4596/97 $25.00

The crystallographic details of the η_1- and η_2-carbide structures are generally attributed to Westgren (15) and Kislyakova (16), respectively. However, the first description of the η-carbide structure by Westgren (15) in 1933 was originally based on a composition of Fe_4W_2C. The existence of this composition was doubted by several researchers since no other known η-carbide compounds exhibit this stoichiometry (19, 20). In addition, the experimental information pertaining to the determination of this assumed chemical formula was somewhat in question, since the composition and structure of these precipitates in commercial steel billets were determined without the benefit of X-ray microprobe and transmission electron microscope analytical methods. Although currently these techniques are routinely used to identify the structure and composition of unknown precipitates, it is likely that the small volume fraction and fine nature of these carbide precipitates found in commercial steels would still render the analysis quite tedious. Recently, however, we have synthesized the nitride analog of this composition, Fe_4W_2N, as a single-phase material in gram quantities using a novel metal-organic synthesis approach. On the basis of careful X-ray diffraction measurements, Rietveld refinement analysis (21), and quantitative chemical analysis, we have determined that the compound indeed crystallizes with a structure which is consistent with that originally described by Westgren for Fe_4W_2C.

EXPERIMENTAL PROCEDURE

In the course of trying to understand the synthesis and structure of various types of ternary transition metal nitrides, we have developed a metal-organic-based synthesis strategy which has proven to be very useful in preparing a number of these compounds, including Fe_3Mo_3N, Ni_3Mo_3N, Ti_3AlN (22), $CrWN_2$ (7), Fe_3W_3N (10), and Co_3W_3N (11). In its current form, the synthesis procedure involves essentially two sequential reaction steps: (1) the formation of a polymeric precursor induced by the complexation of several transition metal chloride species dissolved in acetonitrile and (2) the ammonolysis of the complexed precursor to yield the ternary nitride.

(A) Materials and Equipment

The inorganic metal chlorides, $FeCl_2 \cdot 4H_2O$ (99%, Aldrich) and WCl_6 (99.9 + %, Aldrich), were used as received. The solvent, HPLC-grade acetonitrile (Fisher Scientific), and the complexing agent, triethylamine (99 + %, Sigma), were used without further purification. Electronic-grade ammonia (Matheson Gas) was used for all the pyrolysis and ammonolysis treatments conducted on the mixed-metal precursors. All chemical manipulations were conducted in an argon-filled glovebox (O_2 and $H_2O \leq 5$ ppm; Vacuum Atmospheres) or under a protective stream of ultrahigh purity (UHP) nitrogen unless otherwise noted. All of the glassware used was acid washed with NoChromix and oven dried prior to use.

(B) Precursor Synthesis

The Fe–W metal-organic precursor and Fe_4W_2N compound were prepared using a procedure similar to that which was reported by us for the preparation of other ternary transition metal nitride powders (22). Figure 1 shows a schematic of the procedure followed in this work. Approximately 4- to 10-g quantities of the iron and tungsten chlorides were dissolved in a 2 : 1 stoichiometric molar ratio, respectively, in acetonitrile. Once the chlorides were thoroughly dissolved, triethylamine was added to the solution under vigorous stirring. The amount of triethylamine needed for complexation was determined assuming complete reaction with the chlorine from both metal chloride species by triethylamine. Since the complexation reaction of triethylamine is in general exothermic and some hydrogen chloride gas does evolve, the triethylamine was added at a slow rate of ca. 10 ml/min. In this case, for the Fe–W–N system, the complexation reaction occurs nearly instantaneously as evidenced by rapid changes in the color and viscosity of the acetonitrile solution. Initially a watery, dark transparent brown liquid, the mixed chloride solution, changes to an opaque reddish-brown color and becomes much thicker upon complexing with triethylamine. If allowed to settle, the solution separates into two liquids: a clear acetonitrile-based phase and a viscous opaque brown phase which settles to the bottom of the reaction flask. After the addition of triethylamine was complete, the two-phase solution was shaken by hand to ensure complete reaction and to promote mixing of the different species. The liquid mixture was then heated to evaporate off the acetonitrile, leaving behind a solid dark red-brown amorphous product. This solid was further dried at 120°C under a vacuum for ca. 12 h, after which it was crushed into a powder using an agate mortar and pestle.

(C) Ammonolysis and Pyrolysis

Samples of the powder precursor were weighed into high-purity aluminum nitride crucibles and placed into a $2\frac{1}{2}$-in.-diameter quartz flow-through tube furnace. The back end of the tube furnace was connected to a mineral oil bubbler and the front end was connected to the gas line. Prior to initiating the heat treatment, the tube was purged for 20 min with prepurified nitrogen and then purged for another 10 min with ammonia gas. The powder samples were fired in 120 ml/min flowing ammonia using the following sequence of heat treatment conditions: (1) ramp from room temperature to 120°C at 5°C/min and hold at 120°C

for 1 h, (2) ramp from 120°C to 300°C at 3°C/min and hold at 300°C for 1 h, (3) ramp from 300°C to 950°C at 3°C/min and hold at 950°C for 4 h, and (4) allow the sample to furnace cool. Although the 4-h soak time was long enough to produce a single-phase crystalline compound, the powders were annealed in ammonia for an additional 10–20 h at 950°C to increase the crystallite size and sharpen the X-ray diffraction data prior to the final Rietveld refinement work. As will be discussed, this prolonged annealing treatment often initiated an unintended, but interesting, phase transformation in the nitride material.

(D) Materials Characterization

A quantitative chemical assay was conducted by Galbraith Laboratories (Knoxville, TN) on two samples of the powder product. They employed a wet chemical analysis technique to determine the concentration of the metal species and combustion analyses to evaluate the nitrogen and carbon contents. In preparing samples for X-ray analysis, the powders were mixed with acetone to form a slurry and ground for ca. 15 min using an agate mortar and pestle. The samples were then loaded into standard brass sample holders for X-ray diffraction analysis. These measurements were conducted on a Rigaku θ–θ diffractometer employing graphite-monochromated Cu$K\alpha$ radiation under the following step scan settings: 10–120° range, 0.02° step size, and 15-s collection time. Prior to the diffraction experiments, the diffractometer was aligned using a (100)-oriented silicon single crystal for accurate peak positions.

An initial estimate of the lattice parameter for Fe_4W_2N was obtained by least-squares refinement of the angular

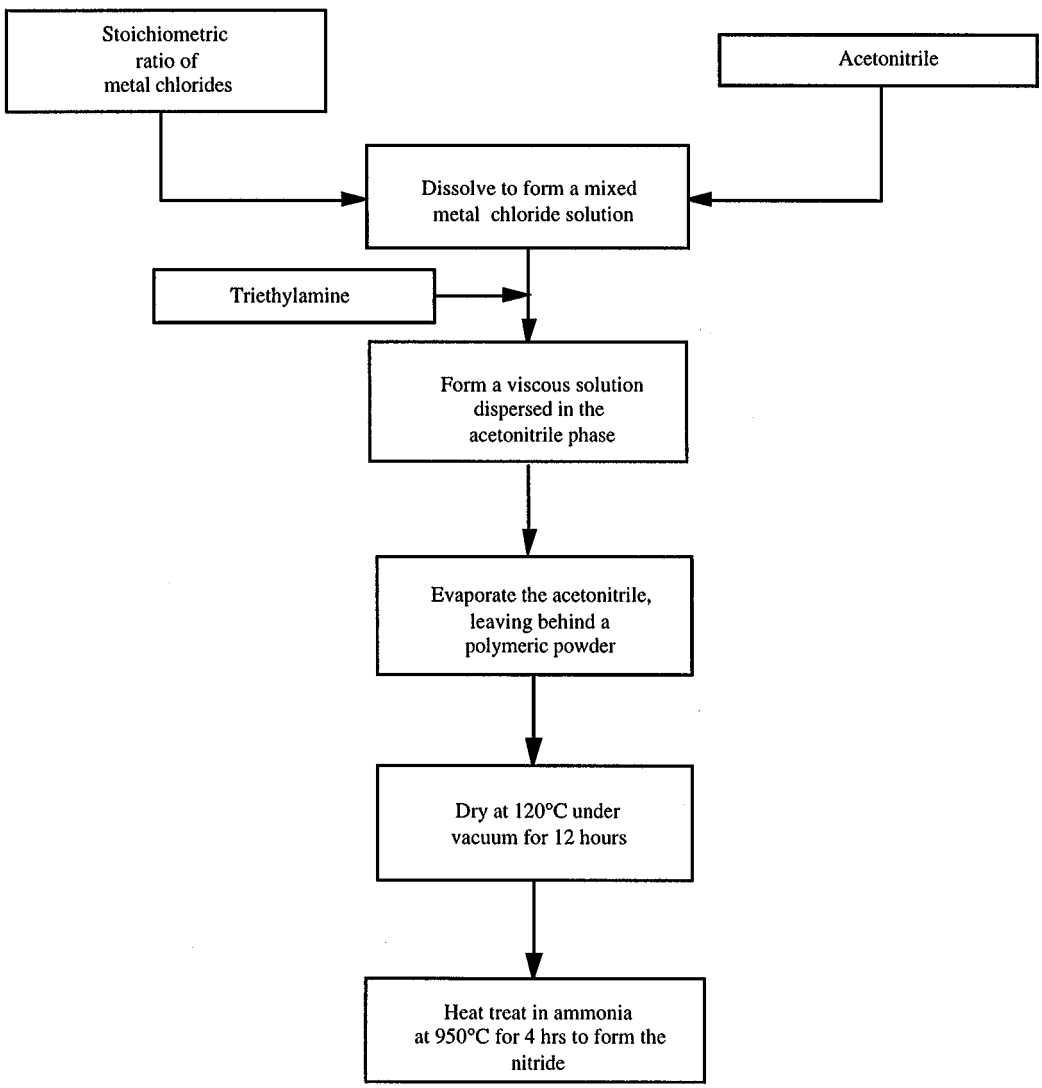

FIG. 1. Flowchart showing the procedure used to synthesize the ternary nitride in this study.

TABLE 1
Chemical Analysis of the Ammonolyzed Fe–W Compound

	Concentration (atom %)		
	Sample 1	Sample 2	Theoretical
Fe	56.98	57.32	57.14
W	28.76	28.48	28.57
N	14.09	14.01	14.29
C	0.097	0.085	

positions of the 25 reflections obtained in the 2θ range $30^\circ \leq 2\theta \leq 85^\circ$. Rietveld refinements were then carried out using the RIETAN-94 (23, 24) program over the entire 10–120° range of the X-ray diffraction data. The profile shape was represented by the modified psuedo-Voigt function (25, 26), with profile asymmetry introduced by employing a multiterm Simpson's rule integration (27). In addition to the profile, lattice, thermal displacement, and structure parameters, the zero-point shift, nine background parameters, and the scale factor were refined without correction for preferred orientation. Thermal vibrations were assumed to be isotropic. Crystal structure graphics and geometric measurements were prepared using the Ca.R.Ine crystallographic software package (28).

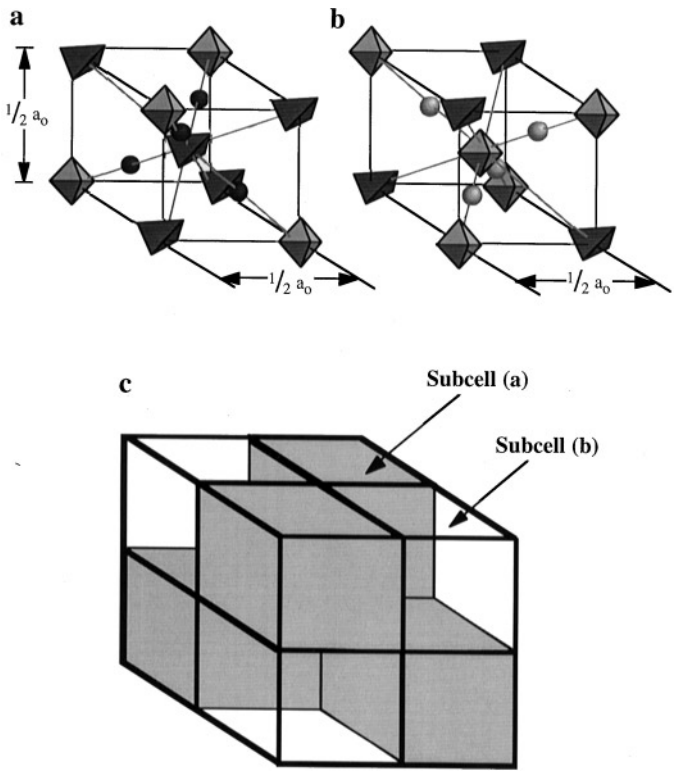

FIG. 2. Schematic representation of the T_4M_2X unit cell (adapted from ref. 33). Although T_4M_2X has a large fcc unit cell, its structure can be visualized as two subcells, (a) and (b), alternately stacked in a cubic array (c), where the dark gray spheres represent T atoms in addition to those in the octahedra and the light gray spheres represent interstitial, X, atoms such as carbon. The patterns in the subcells assume a diamond cubic-type of arrangement in which the T octahedra or the M tetrahedra are centered at the corners and center of these small cubic cells. Note: To show the internal arrangement of the subcells, the octahedra and tetrahedra in this figure have been collapsed about their centers.

TABLE 2
X-ray Powder Diffraction Data of Fe_4W_2N

(h k l)	d spacing (Å)	Relative intensity
1 1 1	6.398	6
2 2 0	3.918	2
3 1 1	3.341	4
2 2 2	3.199	<1
4 0 0	2.770	23
3 3 1	2.542	34
4 2 2	2.262	54
5 1 1	2.133	100
4 4 0	1.959	29
5 3 1	1.873	<1
4 4 2	1.847	3
6 2 0	1.752	1
5 3 3	1.690	<1
6 2 2	1.671	3
4 4 4	1.599	<1
5 5 1	1.552	12
6 4 2	1.481	<1
7 3 1	1.443	4
8 0 0	1.385	2
7 3 3	1.354	10
6 4 4	1.344	<1
8 2 2	1.306	27
5 5 5	1.280	6
6 6 2	1.271	<1
8 4 0	1.239	<1
7 5 3	1.216	1
8 4 2	1.209	<1
6 6 4	1.181	2
9 3 1	1.162	<1
8 4 4	1.131	<1
9 3 3	1.114	7
8 6 2	1.087	5
7 7 3	1.071	5
10 2 2	1.066	<1
9 5 3	1.033	<1
8 6 4	1.029	<1
10 4 2	1.012	<1
11 1 1	0.999	1
8 8 0	0.979	<1
9 5 5	0.968	2
10 4 4	0.964	1
10 6 0	0.950	4
9 7 3	0.940	1
10 6 2	0.937	<1
8 8 4	0.923	3
11 5 1	0.914	3
10 6 4	0.899	7

RESULTS AND DISCUSSION

Results from the chemical analyses, shown in Table 1, verify the stoichiometry of the ammonolyzed Fe–W compound to be Fe_4W_2N. Carbon impurities were found to be present in relatively insignificant concentrations. As seen in other ternary transition metal–transition metal nitrides (6, 7), the nitrogen content of this compound is slightly substoichiometric. Unlike the ternary alkali metal–transition metal nitrides, such as $LiMoN_2$ (29) and Na_3WN_3 (30), Fe_4W_2N appears to be quite stable to moisture and oxygen, as verified by the identical diffraction pattern and constant lattice parameters obtained even after exposure of the compound to ambient atmosphere for several months. The observed d spacings and Bragg intensities determined from the powder XRD pattern for Fe_4W_2N are displayed in Table 2. The pattern was indexed to a face-centered cubic unit cell with a lattice parameter of $a = 11.0810(9)$ Å and systematic absences consistent with those of the $Fd\bar{3}m$ space group. Since the lattice parameter and space group are similar to that reported for many η-carbide compounds, the atomic coordinates of the different variants of this carbide structure were used as the starting point for Rietveld refinements of the new nitride.

As discussed previously, variations in the η-carbide structure can be classified by the metal-to-metal ratio of the compound and the resulting Wyckoff sites each metal atom occupies, as well as the fractional occupancy of the interstitial [8(*a*)–16(*c*)] sites that are filled by the anion. Parthe *et al.* (31) have reviewed the structural data of various carbide and nitride compounds containing T_6X (X = C or N) octahedra. The differences between the η-carbide variants from this study are summarized in Table 3. In this table, the different Wyckoff positions that each element can assume are differentiated by adding a Roman numeral superscript. Note that each derivative of the η-carbide structure is based on a filled version of the Ti_2Ni structure (32). As shown in Fig. 2a–c, separate clusters of T (titanium) and M (nickel) atoms in this structure essentially define two interpenetrating diamond cubic lattices. The T atoms cluster in regular octahedra on the first diamond cubic lattice, while the M atoms can be found in groups of four as tetrahedra on a second diamond lattice which interpenetrates the first through a $\frac{1}{2},\frac{1}{2},\frac{1}{2}$ unit cell translation. Sixteen additional metal atoms, either T- or M-type depending on the $T:M$ ratio, tetrahedrally coordinate the M tetrahedra. In filled versions of Ti_2Ni, depending on the metal-to-nonmetal ratio, eight or more nonmetal atoms surround the T octahedra in tetrahedral coordination. These nonmetal atoms are located centrally between two neighboring T octahedra, producing a sixfold trigonal antiprismatic, or distorted octahedral, environment of T atoms around each nonmetal atom.

TABLE 3
Structural Data of the η-Carbides[a] ($Fd\bar{3}m$)

	Prototype structure	Ideal formula	Examples	Wyckoff positions	Reference
(1)	Unfilled Ti_2Ni type. $T:M:X = 2:1:0$	$T^{\mathrm{I}}_6T^{\mathrm{II}}_2M_4$	$Ti_6Ti_2Ni_4 = Ti_2Ni$	T^{I} in 48(f), $x \sim 0.19$ T^{II} in 16(d) M in 32(e), $x \sim 0.43$	31
(2)	Filled Ti_2Ni type with only one-third of the interstitial sites filled. $T:M:X = 6:6:1$	$T_6M^{\mathrm{I}}_4M^{\mathrm{II}}_2X_1$	$W_6Co_4Co_2C_1 = W_6Co_6C$	T in 48(f), $x \sim 0.19$ M^{I} in 32(e), $x \sim 0.43$ M^{II} in 16(d) X in 8(a)	16
(3a)	Filled Ti_2Ni type with only two-thirds of the interstitial sites filled. $T:M:X = 3:3:1$	$T_6M^{\mathrm{I}}_4M^{\mathrm{II}}_2X_2$	$W_6Fe_4Fe_2C_2 = W_3Fe_3C$	T^{I} in 48(f), $x \sim 0.19$ M^{I} in 32(e), $x \sim 0.43$ M^{II} in 16(d) X in 16(c)	14
(3b)	Filled Ti_2Ni type with only two-thirds of the interstitial sites filled. $T:M:X = 4:2:1$	$T^{\mathrm{I}}_6T^{\mathrm{II}}_2M_4X_2$	$W_6W_2Co_4C_2 = W_4Co_2C$	T^{I} in 48(f), $x \sim 0.19$ T^{II} in 16(d) M in 32(e), $x \sim 0.43$ X in 16(c)	15
(4)	Filled Ti_2Ni type with all of the interstitial sites filled. $T:M:X = 4:2:3/2$	$T^{\mathrm{I}}_6T^{\mathrm{II}}_2M_4X^{\mathrm{I}}_2X^{\mathrm{II}}_1$	$Nb_6Nb_2Zn_4C_2C_1 = Nb_8Zn_4C_3$	T^{I} in 48(f), $x \sim 0.19$ T^{II} in 16(d) M in 32(e), $x \sim 0.43$ X^{I} in 16(c) X^{II} in 8(a)	17

[a]Adapted from ref 31.

Alternative views of the filled Ti_2Ni structure can be visualized using XT_6 octahedra and polyhedral clusters of the remaining atoms. For example, in M_2T_4X the nonmetal atoms are octahedrally coordinated by T atoms, forming slightly distorted XT_6 octahedra, shown in Fig. 3a. On the other hand, the M atoms and remaining T atoms cluster into groups of eight, M_4T_4, arranged into four tetrahedra each which share a face with a fifth central tetrahedron, thus forming a stella quadrangula (34). The M_4T_4 stellae quadrangulae are displayed in Fig. 3b. These octahedral and tetrahedral arrangements are related. The first can be viewed as a set of octahedra ordered such that a central unfilled, regular T octahedron is bounded on four faces (two opposing pairs) by filled, slightly distorted XT_6 octahedra, as shown in Fig. 4. In fact, Fig. 4 directly demonstrates the spatial relationship between the unfilled regular T_6 octahedra in this structure, shown in Fig. 2b, and the filled distorted XT_6 octahedra seen in Fig. 3a. The second, tetrahedral, arrangement of the M atoms and remaining T atoms can be viewed as a central tetrahedron, M_4, capped on all four faces by additional tetrahedra, M_3T, in which the T atoms are at the far-most vertex of each outer tetrahedron. Thus, the XT_6 octahedra corner share in a manner which is similar to that seen in the pyrochlore structure, while the M_4T_4 stellae quadrangulae also corner share, but on a structural lattice separate from that formed by the XT_6 octahedra. Because these two lattices interpenetrate, each occupying the interstices of the other, their unit cell edges are identical in size.

As shown in Table 3, only one of the η-carbide variants, $T^{\mathrm{I}}_6T^{\mathrm{II}}_2M_4X_2$ (3b), has a stoichiometry which matches that of Fe_4W_2N and it would have an anti form relative to the convention discussed above, in which iron (the M atoms) would now rest in the T positions and tungsten (the T atoms) would accordingly sit on the M sites in the new nitride. This would yield the same structure described in the preceding paragraph, except that it contains NFe_6 octahedra and W_4Fe_4 stellae quadrangulae. A second structure which satisfies the new nitride's stoichiometry is one based on 3b, in which the interstitial sites are exchanged such that nitrogen sits on the 16(d) positions and iron on the 16(c) positions. This arrangement, not observed in any known compounds, would yield a structure containing corner-sharing $FeFe_6$ octahedra and corner-sharing N_4W_4 stellae quadrangulae. Two other structures can be considered, based on random mixing of iron and tungsten atoms on the 48(f) site in the 3a structure. The first of these, with an Fe:W ratio of 2:1 on the 48(f) site, would contain $N(\frac{2}{3}Fe,\frac{1}{3}W)_6$ octahedra and Fe_4W_4 stellae quadrangulae. Again, this structure has never been reported as a prototype for any known compounds. The second randomly mixed structure is the disputed Westgren Fe_4W_2C model, which is

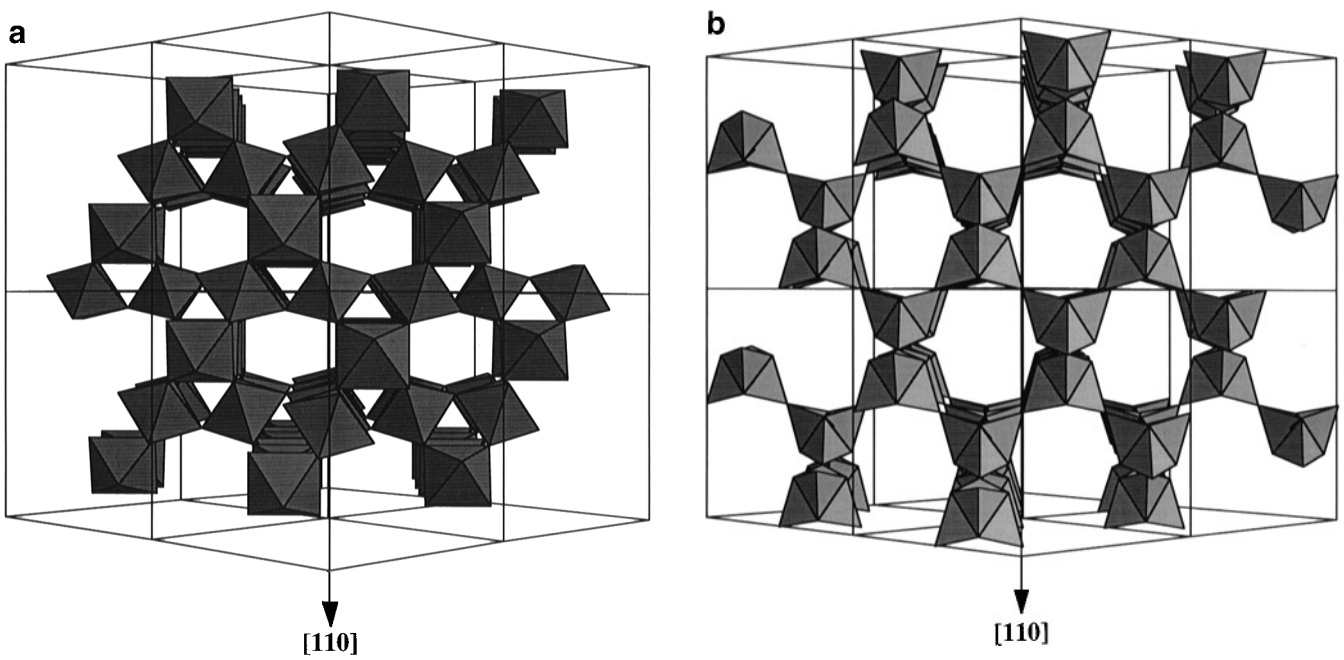

FIG. 3. Polyhedral models of the M_2T_4N η_2-carbide structure. In (a) each nitrogen atom is coordinated by six T atoms, forming slightly distorted NT_6 octahedra. The octahedra share corners in a manner similar to that seen in the pyrochlore structure. In (b), clusters of four M atoms and four T atoms are arranged into four tetrahedra, M_3T, each which share a face with a fifth central tetrahedron, M_4, forming a stella quadrangula. Note that in this structure the T atoms can be found on the four corner-shared vertices of each stella quadrangula. Note: In each of these views, the origin of the unit cell has been shifted by $-\frac{1}{8}, -\frac{1}{8}, -\frac{1}{8}$ for a clearer representation.

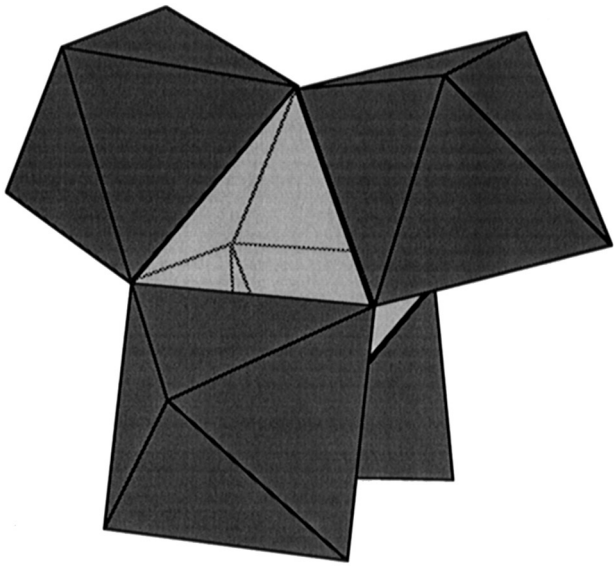

FIG. 4. Octahedral arrangement of the pyrochlore-like lattice in η-carbide structures. Shown sharing corners are four dark gray, slightly distorted XT_6 octahedra. Centered within the XT_6 octahedra is a regular T_6 octahedron, shaded lighter gray (adapted from ref. 34).

TABLE 4
Positional Parameters Initially Proposed for the Possible η-Carbide Structure of Fe_4W_2N

	Atom	Site	x	y	z	Occupancy
(1)	Fe(1)	48(f)	0.1875[a]	0	0	1
	W	32(e)	0.425[a]	0.425	0.425	1
	Fe(2)	16(d)	$\frac{5}{8}$	$\frac{5}{8}$	$\frac{5}{8}$	1
	N	16(c)	$\frac{1}{8}$	$\frac{1}{8}$	$\frac{1}{8}$	1
(2)	Fe(1)	48(f)	0.1875	0	0	1
	W	32(e)	0.425	0.425	0.425	1
	Fe(2)	16(c)	$\frac{1}{8}$	$\frac{1}{8}$	$\frac{1}{8}$	1
	N	16(d)	$\frac{5}{8}$	$\frac{5}{8}$	$\frac{5}{8}$	1
(3)	Fe(1)	48(f)	0.1875	0	0	$\frac{2}{3}$
	W(1)	48(f)	0.1875	0	0	$\frac{1}{3}$
	Fe(2)	32(e)	0.425	0.425	0.425	1
	W(2)	16(d)	$\frac{5}{8}$	$\frac{5}{8}$	$\frac{5}{8}$	1
	N	16(c)	$\frac{1}{8}$	$\frac{1}{8}$	$\frac{1}{8}$	1
(4)	Fe(1)	48(f)	0.1875	0	0	$\frac{1}{3}$
	W	48(f)	0.1875	0	0	$\frac{2}{3}$
	Fe(2)	32(e)	0.425	0.425	0.425	1
	Fe(3)	16(d)	$\frac{5}{8}$	$\frac{5}{8}$	$\frac{5}{8}$	1
	N	16(c)	$\frac{1}{8}$	$\frac{1}{8}$	$\frac{1}{8}$	1

[a]The ideal x parameters for the 48(f) and 32(e) Wyckoff positions in the η-carbide structure are 0.1875 and 0.425, respectively.[34]

also based on the $T_6M^{\mathrm{I}}_4M^{\mathrm{II}}_2X_2$ (3a) variant, with only two-thirds of the T sites randomly occupied by T atoms and the remaining one-third filled with M atoms. In Fe_4W_2N, exhibiting this form, the resulting structure would contain corner-sharing $N(\frac{1}{3}Fe,\frac{2}{3}W)_6$ octahedra and Fe_8 stellae quadrangulae.

Each of these proposed structures for Fe_4W_2N is summarized in Table 4 and labeled 1, 2, 3, or 4, respectively. By simulating the X-ray pattern of each using RIETAN-94, we were able to determine a prospective starting model for the final Rietveld refinement calculations. Listed in Table 5 are the results of this initial analysis, demonstrating an excellent match between the Westgren model (#4) and the experimental data. Using this model, the crystal structure of Fe_4W_2N was refined and the bond lengths for the various nearest-neighbor combinations were calculated to determine the validity of the structure. The refinement converged with $R_{wp} = 12.73\%$, $R_p = 7.09\%$, $R_I = 4.78\%$, and $S = 1.72$. The results of the refinement and the data for the crystal structure and atomic positions are reported in Table 6. Figure 5 shows a comparison of the experimental plot with that obtained by refinement, along with the calculated residuals.

A schematic of the unit cell of Fe_4W_2N similar to the Fe_4W_2C Westgren structure is shown in Fig. 6. Polyhedral representations of the atomic coordination in Fe_4W_2N consistent with the Rietveld refinement and diffraction data are schematically very similar to those shown in Fig. 3a and 3b, except that the composition of the filled, distorted octahedra is $N(\frac{1}{3}Fe,\frac{2}{3}W)_6$ and the composition of the stellae quadrangulae is Fe_8. Again, the $N(\frac{1}{3}Fe,\frac{2}{3}W)_6$ octahedra corner share in a manner similar to that seen in the pyrochlore structure, while the Fe_8 stellae quadrangulae also corner share on a diamond cubic structural lattice which is translated by a $\frac{1}{2},\frac{1}{2},\frac{1}{2}$ unit cell vector relative to the lattice formed by the octahedra.

Selected bond distances and angles are listed in Table 7. The metal–metal and metal–nitrogen bond distances determined for Fe_4W_2N are similar to those found in other ternary transition metal nitrides and carbides belonging to this family. The M–N bond distance in Fe_4W_2N of

TABLE 5
Calculated Intensities[a] of the First 10 Bragg Peaks in the Possible η-Carbide Structures of Fe_4W_2N

Structure type[b]	111	220	311	222	400	331	422	511	440	531
(1)	100	30	18	16	3	1	17	100	9	5
(2)	45	34	58	17	3	9	19	100	10	1
(3)	25	0	10	28	1	53	36	100	40	8
(4)	9	1	3	0	18	33	57	100	18	0
Experimental	6	2	4	0	23	34	54	100	29	0

[a]The Bragg intensities for each of the structures in Table 4 were calculated using the structure simulation option available in RIETAN-94.[23,24] For these calculations, the isotropic thermal parameter, B_{iso}, was assigned a value of 1 for each atom.

[b]From Table 4.

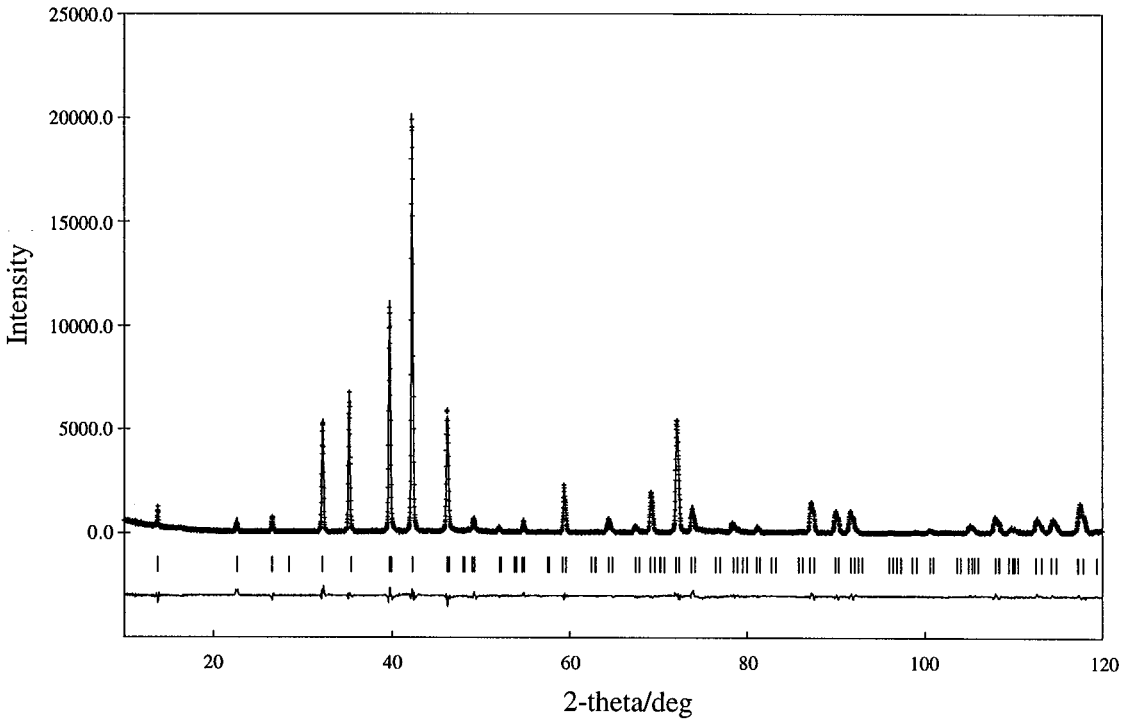

FIG. 5. Observed (crosses) and calculated (solid) X-ray diffraction profiles for Fe_4W_2N. Tic marks below the diffractogram represent the allowed Bragg reflections. The residual line is located at the bottom of the figure.

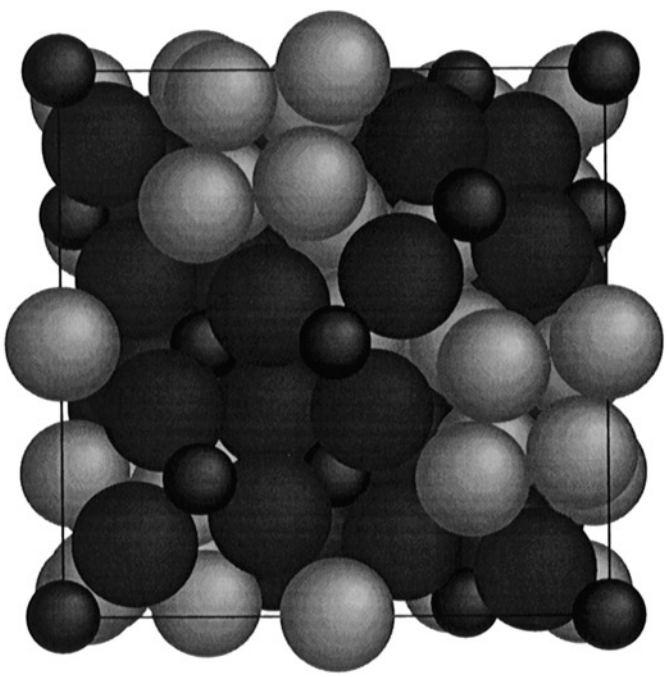

FIG. 6. Proposed unit cell structure of Fe_4W_2N: the dark gray, large spheres represent a random mixture of tungsten and iron atoms in a 2:1 ratio, the light gray, medium-size spheres represent additional iron atoms, and the small, light gray spheres represent the nitrogen atoms. Note: In each of these views, the origin of the unit cell has been shifted by $-\frac{1}{8}, -\frac{1}{8}, -\frac{1}{8}$ for a clearer representation.

2.103(3) Å compares well with that for the analogous W–N bonds in Fe_3W_3N, 2.119(5) Å (10) and Co_3W_3N, 2.119(1) Å (11). Likewise, the *M*–*M* bond distances in Fe_4W_2N of 3.041(7) and 2.905(5) Å are similar to the W–W separations found in Fe_3W_3N, 3.090(5) and 2.901(2) Å (10), and in Co_3W_3N, 3.094(1) and 2.896(4) Å (11). Similarly, the Fe–Fe bond distances of Fe_4W_2N are very nearly equal to those of Fe_3W_3N (10) and Fe_3W_3C (13). The metal–nitrogen bond lengths in these ternary transition metal nitrides are significantly longer in comparison to bond lengths existing in the alkali metal–transition metal and alkaline-earth metal–transition metal nitrides. For example, the W–N bond distances in Na_3WN_3 (31) and Ba_3WN_4 (36) range from 1.78(1) to 1.93(1) Å, nearly 10–20% shorter than the *M*–N bonds in Fe_4W_2N. The longer metal–nitrogen bond lengths imply that the bonding in Fe_4W_2N is at least partially covalent. Similarly, comparisons of the metallic bond lengths in the $N(\frac{1}{3}Fe,\frac{2}{3}W)_6$ octahedra with those in metallic tungsten and iron suggest that the longer metallic bonds in Fe_4W_2N are due to covalent bonding in the octahedra. On the other hand, the Fe–Fe bond lengths in Fe_4W_2N are nearly equivalent to that found in metallic iron, suggesting that within the Fe_8 stellae quadrangulae clusters, the iron atoms form metallic bonds.

Many of the η-carbide compounds that have been studied previously, such as Fe_6Mo_6C (37), are quite refractory, showing excellent stability at elevated temperatures. In

TABLE 6
Results of the X-Ray Rietveld Refinement for Fe_4W_2N in Space Group $Fd\bar{3}m$

Formula weight	605.09
a (Å)	11.0810(9)
V (Å^3)	1360.6(5)
Z	16
D_{calc} (g/cm^3)	11.816
Powder color	Black
X-ray radiation (λ)	Cu$K\alpha$
Monochromator	Graphite (0002)
2θ range (deg)	10.0–120.0
Scan step size (deg)	0.02
Count time (s/step)	15
Test temperature (°C)	23 ± 1
No. of reflections	47
No. of profile parameters	20
No. of structure parameters	7
Reliability factors[a]	
R_{wp}	0.1273
R_p	0.0709
R_I	0.0478
S	1.72

Atomic parameters for Fe_4W_2N

Atom	Wyckoff	x	y	z	B_{iso} (Å)	Occupancy
W	48(f)	0.194(1)	0	0	0.5(8)	$\frac{2}{3}$
Fe(1)	48(f)	0.194(1)	0	0	0.5(8)	$\frac{1}{3}$
Fe(2)	32(e)	0.426(8)	0.426(8)	0.426(8)	0.3(3)	1
Fe(3)	16(d)	$\frac{5}{8}$	$\frac{5}{8}$	$\frac{5}{8}$	1.1(3)	1
N	16(c)	$\frac{1}{8}$	$\frac{1}{8}$	$\frac{1}{8}$	1.6(6)	1

[a]Defined as follows: $R_{wp} = \{[\sum W_i(Y_{obs} - Y_{cal})^2/(\sum W_i(Y_{obs})^2)]\}^{1/2}$; $R_p = (\sum|Y_{obs} - Y_{cal}|)/(\sum Y_{obs})$; $R_I = (\sum|I_{obs} - I_{cal}|)/(\sum I_{obs})$; and $S = R_{wp}/R_e$.

contrast, Fe_4W_2N surprisingly appears to decompose or change phase upon annealing at the nitride formation temperature of 950°C. As shown in Fig. 7, the cubic η-carbide phase, which we have identified stoichiometrically as Fe_4W_2N, is metastable at 950°C. However, the phase transformation does not occur, due to either sluggish diffusional kinetics or a small reaction energy, until the material has been held at temperature for ca. 20 h. As seen in Fig. 7b, the primary phase after annealing in NH_3 for 20 h is still the η-carbide compound. Based on their d spacings, the secondary peaks observed in the XRD pattern have been tentatively been attributed to a layered ternary nitride compound, with a structure that is expected to be similar to that of $FeWN_2$ (6) or $CrWN_2$ (7). At this point, the stoichiometry of this phase has not yet been identified. To date, we have annealed these powders for as long as 40 h, finding that they do not completely transform from the η-carbide structure over this period of time (see Fig. 7c). We hope to eventually isolate enough of the transformed product to conduct X-ray diffraction and chemical analyses or, alternatively, identify its structure and stoichiometry through a combination of electron diffraction and X-ray and electron spectroscopy.

TABLE 7
Selected Bond Distances and Angles in Fe_4W_2N

Bond distances (Å)			Bond angles (°)		
Fe(2)–Fe(2)	2.2943(3)	3×	M–N–M	87.3(3)	2×
Fe(2)–M[a]	2.822(3)	3×	M–N–M	92.6(7)	2×
Fe(2)–M	2.777(3)	3×	M–N–M	180.0(0)	3×
Fe(2)–N	3.441(4)	3×	M–N–M	90.0(0)	8×
Fe(3)–Fe(3)	3.917(8)	12×	N–W–N	137.2(4)	2×
Fe(3)–Fe(2)	2.341(5)	6×	M–Fe(3)–M	62.4(5)	6×
Fe(3)–W	2.802(8)	6×	M–Fe(2)–M	66.4(2)	3×
N–Fe(3)	3.917(8)	12×	M–Fe(2)–M	63.7(5)	3×
N–N	3.917(8)	12×	Fe(3)–Fe(2)–Fe(3)	66.4(0)	3×
N–M	2.103(3)	6×	Fe(2)–Fe(3)–Fe(3)	58.5(9)	6×
M–M	3.041(7)	4×	Fe(2)–Fe(2)–Fe(2)	60.0(0)	3×
M–M	2.905(5)	4×			

[a]Where statistically, $M = 1/3\text{Fe} + 2/3\text{W}$.

CONCLUSIONS

We have synthesized a new ternary transition metal nitride, Fe_4W_2N, by the ammonolysis of a solution-derived, polymeric metal-organic precursor at 950°C. This nitride is found to be isostructural with the Westgren Fe_4W_2C η-carbide structure, crystallizing in a face-centered cubic structure. Three distinct iron sites exist in this compound, the first of which is the 48(f) site containing a random mixture of iron and tungsten atoms, in a ratio of 1:2, arranged in octahedral clusters. The iron atoms sitting on the 32(e) sites form tetrahedral clusters. These two distinct polyhedral arrangements order on separate diamond cubic lattices, which differ only a $\frac{1}{2},\frac{1}{2},\frac{1}{2}$ unit cell translation. Sixteen additional iron atoms, Wyckoff position 16(d), are tetrahedrally coordinated around the iron tetrahedra and sixteen nitrogen atoms surround the mixed iron–tungsten octahedra in tetrahedral coordination. The nitrogen atoms are located centrally between any two octahedra, producing a sixfold trigonal antiprismatic environment of metal atoms around each nitrogen atom. Alternatively, Fe_4W_2N can be described in terms of coordination polyhedra in which the nitrogen atoms are octahedrally coordinated by the random iron–tungsten mixture, forming $N(\frac{1}{3}Fe,\frac{2}{3}W)_6$ octahedra, while the remaining iron atoms cluster in sets of eight, forming stellae quadrangulae. The $N(\frac{1}{3}Fe,\frac{2}{3}W)_6$ octahedra share common corners in a manner similar to that seen in the pyrochlore structure. The Fe_8 stellae quadrangulae also corner share on a structural lattice separate from that formed by the $N(\frac{1}{3}Fe,\frac{2}{3}W)_6$ octahedra. Based on the interatomic distances in Fe_4W_2N, it is suggested that the octahedrally coordinated metal atoms surrounding each nitrogen atom covalently bond with the nitrogen, while the iron atoms in the stellae quadrangulae clusters form metallic bonds.

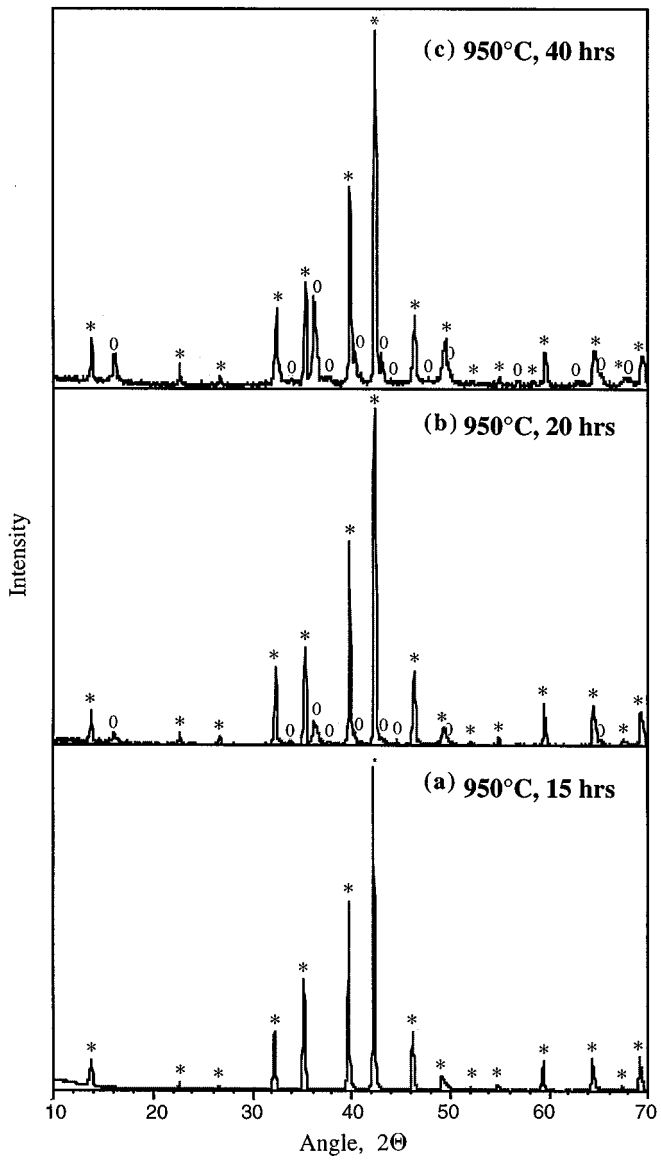

FIG. 7. X-ray diffraction patterns collected on powder samples annealed in ammonia at 950°C for (a) 15, (b) 20, and (c) 40 h. Peaks marked with an asterisk can be assigned to the η-carbide structure, while peaks marked with an "○" represent a second phase, tentatively thought to be a layered nitride structure.

ACKNOWLEDGMENTS

This work is supported by the National Science Foundation under Grants DMR 9301014 and CTS-9309073 and ARPA (Contract N00014-94-1-0773). K.S.W. also acknowledges the support of the Department of Defense in the form of an NDSEG Fellowship.

REFERENCES

1. D. A. Vennos, M. E. Badding, and F. J. DiSalvo, *Inorg. Chem.* **29,** 4059 (1990).
2. H. Jacobs and E. von Pinkowski, *J. Less-Common Met.* **146,** 147 (1989).
3. A. Gudat, S. Haag, R. Kniep, and A. Rabenau, *J. Less-Common Met.* **159,** L29 (1990).
4. J. D. Houmes, D. S. Bem, and H.-C. zur Loye, *in* "MRS Symposium Proceedings: Covalent Ceramics II: Non-Oxides" (A. R. Barron, G. S. Fischman, M. A. Fury, and A. F. Hepp, Eds.), Vol. 327, p. 153. Materials Research Society, Boston, 1993.
5. J. Grins, P.-O. Kall, and G. J. Svensson, *J. Mater. Chem.* **5,** 571 (1995).
6. D. S. Bem, C. M. Lampe-Onnerud, H. P. Olsen, and H.-C. zur Loye, *Inorg. Chem.* **35,** 581 (1996).
7. K. S. Weil and P. N. Kumta, *J. Solid State Chem.* **128,** 2 (1997).
8. P. S. Herle, N. Y. Vasanthacharya, M. S. Hegde, and J. Gopalakrishnan, *J. Alloys Compd.* **217,** 22 (1995).
9. D. S. Bem, J. D. Houmes, and H.-C. zur Loye, *in* "Materials Science Forum: Soft Chemistry Routes to New Materials: Chimie Douce" (J. Rouxel, M. Tournoux, and R. Brec. Eds.), Vols. 152–153, p. 183. Trans Tech Publications, Switzerland, 1993.
10. K. S. Weil and P. N. Kumta, *Acta Crystallogr.*, in press.
11. K. S. Weil and P. N. Kumta, *J. Alloys Compd.*, in press.
12. D. S. Bem, C. P. Gibson, and H.-C. zur Loye, *Chem. Mater.* **5,** 397 (1993).
13. A. Westgren and G. Phragmen, *Trans. Am. Soc. Steel Treat.* **13,** 539 (1928).
14. K. Kuo, *Acta Metall.* **1,** 301 (1953).
15. A. Westgren, *Jern. Ann.* **117,** 1 (1933).
16. E. N. Kislyakova, *J. Phys. Chem. (U.S.S.R)* **17,** 108 (1943).
17. Z. Bojarski and J. Leciejewicz, *Arch. Hutn. Polska* **12,** 255 (1967).
18. W. Jeitschko, H. Holleck, H. Nowotny, and F. Benesovsky, *Monatsh. Chem.* **95,** 1004 (1964).
19. H. H. Stadelmaier, *in* "Developments in the Structural Chemistry of Alloy Phases" (B. C. Giessen, Ed.), p. 141. Plenum Press, New York, 1969.
20. H. J. Goldschmidt, "Interstitial Alloys," p. 88. Plenum Press, New York, 1967.
21. H. M. Rietveld, *J. Appl. Crystallogr.* **2,** 65 (1969).
22. K. S. Weil and P. N. Kumta, *Mater. Sci. Eng. B* **38,** 109 (1996).
23. F. Izumi, *in* "The Rietveld Method" (R. A. Young, Ed.), Chap. 13. Oxford University Press, Oxford, 1993.
24. Y.-I. Kim and F. Izumi, *J. Ceram. Soc. Jpn.* **102,** 401 (1994).
25. P. Thompson, D. E. Cox, and J. B. Hastings, *J. Appl. Crystallogr.* **20,** 79 (1987).
26. R. A. Young, *in* "The Rietveld Method" (R. A. Young Ed.), Chap. 1. Oxford University Press, Oxford, 1993.
27. C. J. Howard, *J. Appl. Crystallogr.* **15,** 615 (1982).
28. C. Boudias and D. Monceau, Ca.R.Ine Cristallographie, version 3.0, 1989.
29. S. H. Elder, L. H. Doerrer, F. J. DiSalvo, J. B. Parise, D. Guyomard, and J. M. Tarascon, *Chem. Mater.* **4,** 928 (1992).
30. D. Ostermann, U. Zachwieja, and H. Jacobs, *J. Alloys Compd.* **190,** 137 (1992).
31. E. Parthe, W. Jeitschko, and V. Sadagopan, *Acta Crystallogr.* **19,** 1031 (1965).
32. G. A. Yurko, J. W. Barton, and J. G. Parr. *Acta Crystallogr.* **12,** 909 (1959).
33. M. H. Mueller and H. W. Knott, *Trans. Met. Soc. AIME* **227,** 674 (1963).
34. H. Nyman, S. Andersson, B. G. Hyde, and M. O'Keeffe, *J. Solid State Chem.* **26,** 123 (1978).
35. Z. Bojarski and J. Leciejewicz, *Struct. Rep.* **32A,** 45 (1967).
36. A. Gudat, P. Hohn, R. Kniep, and A. Rabenau, *Z. Naturforsch. B* **46,** 566 (1991).
37. R. K. Sadangi, B. H. Kear, and L. E. McCandlish, *Powder Met.* **37,** 277 (1994).